# Possible control of plasma transport in the near-Earth plasma sheet via current-driven Alfvén waves (f f H+ )

O. Le Contel, A. Roux, S. Perraut, R. Pellat, Ø. Holter, A. Pedersen, A. Korth

JOURNAL OF GEOPHYSICAL RESEARCH, VOL. 106, NO. A6, PAGES 10,817–10,827, JUNE 1, 2001

# Possible control of plasma transport in the near-Earth plasma sheet via current-driven Alfvén waves ($f \simeq f_{H+}$)

O. Le Contel[1], A. Roux[1], S. Perraut[1], R. Pellat[2], Ø. Holter[3], A. Pedersen[3], and A. Korth[4]

**Abstract.** Two time periods, each covering both quiet and disturbed conditions (growth phase, breakup, and postbreakup phase), are studied. Electric and magnetic field measurements, carried out in the near-Earth plasma sheet (NEPS), are used to calculate the two components (radial and azimuthal) of the electric $\mathbf{E} \times \mathbf{B}/B^2$ drift. These calculations are compared with independent estimates of the ion flow direction deduced from ion flux measurements. During active periods, the two flow directions coincide to a large degree. Evidence is given for two regimes of transport: (1) During the growth phase, and after the active phase, the electric field (radial and azimuthal) and hence the azimuthal and radial flow velocities are small in the near-equatorial region. This is interpreted as the consequence of an electrostatic field that tends to shield the induced electric field associated with time-varying external conditions. (2) During active phases (breakup and pseudobreakup), however, large-amplitude bursts in $\mathbf{E} \times \mathbf{B}/B^2$ radial and azimuthal components (interpreted as flow bursts), with typical velocities of the order of 100 km s$^{-1}$, are observed. The direction of these flow bursts is somewhat arbitrary, and in particular, for the two substorm events described here, sudden reversals in the flow direction are observed. These fast flow bursts coincide with intense low-frequency electromagnetic fluctuations: current-driven Alfvén waves (CDA waves) with frequency $f \simeq f_{H+}$, the proton gyrofrequency. CDA waves produce "anomalous" collisions on timescales shorter than the electron bounce period, thus violating the second adiabatic invariant for electrons. As a consequence, the electrostatic shielding is destroyed, which leads to enhanced radial transport. Thus the transport in the NEPS seems to be controlled by a microscopic current-driven instability.

## 1. Introduction

The process by which the plasma is transported in the Earth's plasma sheet is critical for an understanding of plasma sheet dynamics. There is as yet no consensus about its nature. It is often assumed that the magnetosphere is in a steady state, with a static magnetospheric electric field (derived from a scalar potential) driving a steady earthward "convective" flow, in particular during the substorm growth phase. Using Geotail data, *Nakamura et al.* [1994] have conducted a survey of slow and fast flows. While slow flows ($|V| < 300$ km s$^{-1}$) were observed most of the time, with no preferred direction, transient bursts of fast flows ($|V| > 300$ km s$^{-1}$), are essentially radial with a higher occurence rate earthward (at least inside of 25 $R_E$, $R_E$ being the Earth radius). *Angelopoulos et al.* [1992] have also analyzed these fast flow bursts and termed them bursty bulk flows (BBFs), suggesting that most of the radial flux transport in the plasma sheet could be accomplished by these short-duration, intense flow bursts. These measurements are consistent with what *Kennel* [1995] called a bimodal plasma sheet flow, to stress the difference between the morphology of fast and slow flows. The standard convection models, based on constant electrostatic electric fields, do not describe this complex bimodal regime and are not consistent with the corresponding high temporal variability. Thus "one wonders if steady uniform convection has ever been found" [*Kennel*, 1995, p. 22]. In the present paper we show that there are two regimes of transport in the near-Earth plasma sheet (NEPS), and that the level of ultra low-frequency (ULF) fluctuations, at frequencies of the order of the proton gyrofrequency, seems to control the transition between these regimes.

[1]Centre d'Etude des Environnements Terrestre et Planétaires, Vélizy, France.
[2]Commissariat à l'Énergie Atomique, Paris, France.
[3]Department of Physics, University of Oslo, Oslo, Norway.
[4]Max–Planck–Institut für Aeronomie, Katlenburg–Lindau, Germany.



Paper number 2001JA900013.
0148-0227/01/2001JA900013$09.00

The correlation between ULF waves at $f \geq f_{H+}$ and breakup has been reported by *Lui et al.* [1990, 1992], *Perraut et al.* [1993], and *Shinohara et al.* [1998]. Lui et al. suggested that the waves they observed on AMPTE/CCE result from a cross-field streaming instability. Shinohara et al. invoked a lower hybrid drift instablity to interpret the Geotail data.

In the present paper we investigate the plasma transport in the NEPS, by employing data from several instruments on board the geostationary satellite GEOS 2. In section 2 we compare the direction of the electric drift velocity with the direction of the ion velocity deduced from the azimuthal asymmetry of the ion flux. We also investigate the relation between the various substorm phases and the presence/absence of a substantial earthward plasma flow across the magnetic field. The relation between flow bursts and the level of ULF electromagnetic fluctuations at frequencies of the order of the proton gyrofrequency is considered in section 3. In section 4 we propose a new interpretation for the existence of two regimes of transport and an explanation for the relation between the power in ULF fluctuations and the plasma transport.

## 2. Relation Between Fast Flows and Substorms

### 2.1. Observations in the NEPS

GEOS 2 carried complementary instruments for wave and particle measurements. For the present study we use particle data from the energetic particle instrument (ions from 27 to 400 keV [*Korth et al.*, 1978]), together with data from the wave instrument, and the fluxgate magnetometer (for a detailed description of these instruments, see *Knott* [1975]). Electric field measurements were made with a double probe consisting of two spheres supported by two wire booms which were separated by 42 m. The magnetic fluctuations were measured with a triaxial search-coil magnetometer. In the ULF range studied here, one electric and three magnetic components were measured continuously, in wave form, from 0 to 11 Hz. Signals lasting much more than one spin period (6 s) can be considered as quasi-stationary during one spacecraft rotation; hence two components of the electric field in the spin plane (essentially the equatorial $V, D$ plane, $V$ being directed radially outward and $D$ eastward) can be deduced [*Pedersen et al.*, 1985]. The spin axis is essentially along the $H$ axis, perpendicular to the $V, D$ plane which approximately coincides with the plane of rotation of the electric field antenna. For the present study we have selected two time periods: (1) January 25, 1979, from 2010 UT to 2050 UT (Figure 1a), and (2) January 26, 1979, from 1925 UT to 1955 UT (Figure 2a). Figures 1a and 2a display the three magnetic components $B_H$, $B_V$, and $B_D$. The substorm onset time at GEOS 2 is defined by the start of the increase in the magnetic $B_H$ component. The increases occur at 2018 UT for event 1 and at 1935 UT for event 2. The change in the magnetic configuration is also characterized by fast variations in the other magnetic components. For event 1 the $B_V$ component starts decreasing at about 2017 UT, 1 min before the start of the increase in $B_H$ (2018 UT). For event 2 there is an intensification in the $B_V$ (to more positive) and $B_D$ (to more negative) components, at about 1933-1934 UT, about 1 or 2 min before the sharp increase in $B_H$ (1935 UT). The general field and particle behavior for these two events is described by *Roux et al.* [1991] (event 1), and by *Perraut et al.* [2000] (both events).

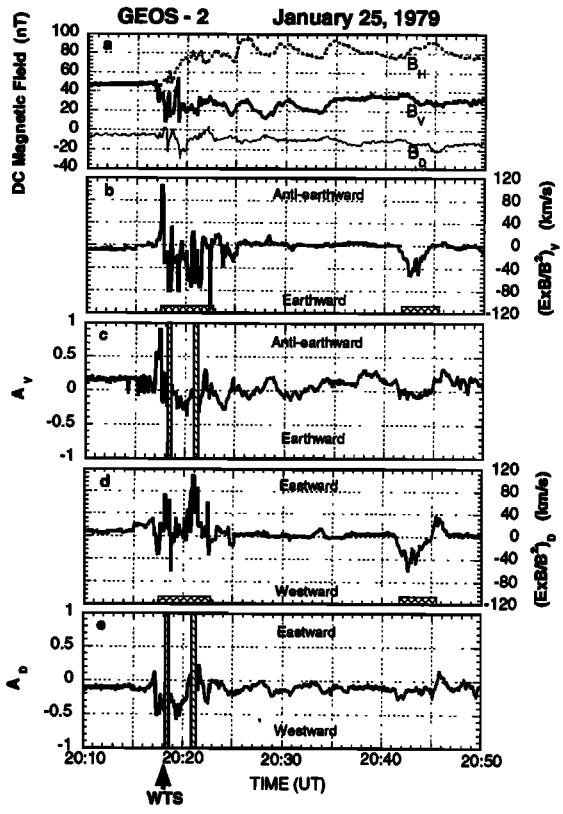


**Figure 1.** January 25, 1979: composite view showing (a) three components ($B_V$, $B_D$, $B_H$) of the magnetic field, (b) the radial $V$ component of the electric drift, (c) $A_V$, the azimuthal asymmetry in the energetic ions flux projected along $V$, (d) the azimuthal $D$ component of the electric drift (e) $A_D$, the azimuthal asymmetry in the energetic ions flux projected along $D$. Figures 1c and 1e display shaded areas which indicate problematic data (see text for more details (subsection 2.5)).

### 2.2. Observations Near the GEOS 2 Magnetic Footprint

The two periods quoted above were selected because all-sky camera pictures from two ground stations, Kevo and Kilpisjärvi, respectively, located east and west of the magnetic footprint of GEOS 2 (as calculated from Tsyganenko T87 model for $Kp = 3$), were available

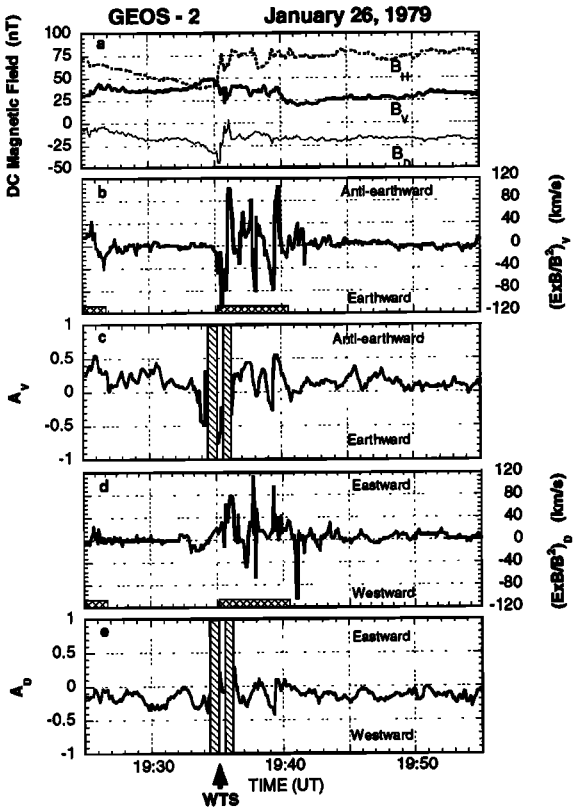


**Figure 2.** Same as Figure 1 for January 26, 1979.

with a 20 s time resolution (see *Roux et al.* [1991] for event 1 and *Perraut et al.* [2000] for event 2). By combining the optical observations from these two stations, it could be shown that before 2017:40 UT there was only a quiet arc in the (clear) sky for event 1. The explosive intensification of the first arc occurred at about 2018 UT (see arrow on the bottom of Figure 1), and developed as a westward traveling surge (WTS). Event 2, at 1935:20 UT, is more complex because it was preceded by a weaker substorm at about 1917 UT. However, a tail-like configuration was recovered at 1930 UT, and a quiet arc was observed on the ground from 1930 UT to 1935:20 UT. The explosive intensification occurred between 1935:20 UT and 1936 UT (see arrow on the bottom of Figure 2), when a newly formed WTS reaches the GEOS 2 footprint. The coincidence between the start of the brightenings of the WTSs, on the ground, and the magnetic signatures of the current disruption at GEOS 2 suggests that GEOS 2 was very close to the substorm onset regions.

### 2.3. Electric Drift Velocity

With the double probe on GEOS 2, the direction and the amplitude of the electric field, projected onto the spin plane, can only be obtained for signals with characteristic time of variation longer than the spin period. During the most active phase of substorm breakup, however, this standard method may fail because the level of fluctuations within a spin period may become as large as, or even larger than, that of the quasi-steady electric field. For these short time intervals it was necessary to estimate the quasi-dc $E$ field by filtering out higher frequency fluctuations.

The electric drifts thus obtained are shown in Figures 1 and 2 for the two events under consideration, respectively. Figures 1b and 2b show the radial components, and Figures 1d and 2d show the azimuthal components of the electric drift. The drift velocities are small before and after the two substorms events, except for short periods around 2043 UT for event 1 and around 1926 UT for event 2, respectively. We will return to these two short periods in section 3. Apart from these two short periods, large values of the electric drift velocity are only found during the breakup, that is, between 2017 UT and 2022 UT for event 1, and between 1935 UT and 1941 UT, for event 2. In both cases, flow reversals are observed. For event 1 the drift changes from antiearthward to earthward and from westward to eastward around 2018 UT, when the first WTS is observed. Around 2021 UT the velocity is directed strongly earthward and eastward, when a second discrete auroral form is observed near the GEOS 2 footprint [*Roux et al.*, 1991]. For event 2 the electric drift changes from earthward to antiearthward (with a weaker eastward component) around 1936 UT, and keeps reversing sign until 1941 UT. For both events the maximum electric drift velocities are of the order of 100 km s$^{-1}$.

### 2.4. Azimuthal Asymmetry in the Ion Flux

The full determination of the ion velocity requires an integration over the whole distribution function; it is, however, not possible for the present events to carry out this computation, because the azimuthal distribution of low-energy ions is not available. Yet, some information can be extracted from the modulation in the flux of energetic ions perpendicular to the magnetic field [*Walker et al.*, 1976; *Mitchell et al.*, 1986]. In a detector head mounted perpendicular to the magnetic field on a spinning spacecraft, the azimuthal asymmetry (AA hereafter) can be due to (1) an $\mathbf{E} \times \mathbf{B}$ drift flow or (2) an ion pressure gradient. Both effects result in azimuthal flux modulation of the integral ion flux while the spacecraft rotates. When the differential fluxes (as function of the energy) are available, the two effects can be distinguished because they have different energy dependence for the AA. Since the effect of the electric drift is energy independent, the modulation is more easily observed for energies below the thermal energy, which for ions is typically 10-20 keV at the GEOS 2 orbit. Conversely, the AA associated with a pressure gradient (and hence with a diamagnetic current) varies with the particle energy because it depends on the ratio $r_L/L_p$ between the ion Larmor radius $r_L$ and the pressure gradient scale length $L_p$. Since $r_L$ is proportional to the

ion velocity, the AA driven by a pressure gradient is a priori more easily detectable for the most energetic ions. Thus it is possible, in principle, to distinguish between the two effects on the basis of the energy dependence of the AA [*Mitchell et al.*, 1986]. On GEOS 2 the AA in the differential flux of energetic ions was measured from 27 to 400 keV, with a time resolution of 1 min. Thus the distinction between the two types of drift can be made. In the present paper, however, we are concerned with perturbations with a timescale shorter than 1 min. Therefore we have used the integrated flux (above 27 keV), which is measured every 5.5 s. Yet, we will see in section 2.5 that it is possible to identify the source of the asymmetry by comparison with measurements of the electric field.

Some of the previous studies, based on the guiding center approach, investigated the asymmetry of the energetic ion flux in the $D$ direction to determine the motion of the trapping boundary [*Walker et al.*, 1976; *Sauvaud and Winckler*, 1980] or the location of the acceleration region [*Ohtani et al.*, 1992]. The guiding center approach, however, does not allow a study of motions which are too fast; the characteristic time $T_c \simeq 2r_L/v_{av}$ ($v_{av}$, being the average velocity of the flow) has to be longer than the time resolution of the measured flux. With an average energy of ions of 30 keV and the time resolution of the ion integral flux being 5.5 s, we obtain an upper limit for the velocity equal to 90 km s$^{-1}$. The electric drift, measured here, can reach 120 km s$^{-1}$ and therefore exceeds the above limit. Furthermore, it is difficult to study the radial plasma motion from the AA of the ion flux in the $D$ direction, due to the important effects of the radial pressure gradient as discussed above. Indeed, by studying the substorm growth phase from the same kind of data, *Pu et al.* [1992] showed that the diamagnetic velocity associated with the ion pressure gradient is generally directed westward and dominates the effect of the electric drift. Conversely, they found that the pressure gradient in the $D$ direction (east/west) is small and gives a negligible diamagnetic velocity. Similarly, the magnetic-curvature drift, which amounts to several kilometers per second in the $D$ direction, is negligible in the $V$ direction.

Aboard GEOS 2 the ion flux, integrated between 27 and 400 keV for pitch angles $\simeq 90°$ (between 60° and 120°), is measured in 18 bins of 20° each, with a time resolution of 5.5 s. We have projected the ion flux measured perpendicular to the magnetic field in each azimuthal bin along the $V$ and $D$ directions, respectively, and summed the corresponding contributions within each spin. We refer to the fluxes of particles coming from positive and negative $V$ ($D$) direction as $F_{V+}$ and $F_{V-}$ ($F_{D+}$ and $F_{D-}$), respectively. We define the asymmetry in the $V$ ($D$) direction as $A_V = (F_{V+} - F_{V-}) / [(F_{V+} + F_{V-})/2]$ ($A_D = (F_{D+} - F_{D-}) / [(F_{D+} + F_{D-})/2]$).

Figures 1c and 1e show $A_V$ and $A_D$, the AA in the flux of energetic ions projected in the radial and azimuthal directions, respectively, before, during, and after the substorm on January 25, 1979. During the growth phase, from 2010 UT to 2017 UT (the growth phase started at 1930 UT), there is a weak AA antiearthward and westward. As discussed above, this AA is likely to be due to a spatial gradient in the energetic ion pressure, at least for the westward component that could correspond to an earthward pressure gradient (i.e., more ions with guiding centers earthward than antiearthward). The typical scale of this gradient is $L_p \sim 5 - 10\ r_L$, corresponding to a few thousand kilometers [*Pu et al.*, 1992]. Taking into account that the magnetic field configuration is highly stressed during the substorm growth phase, such a gradient is expected, and supports the westward directed tail current. During the active period (2017 UT to 2022 UT), $A_V$ and $A_D$ are highly variable both in magnitude and direction, and are 1 order of magnitude larger than during the growth phase. The largest values are along $V$, with a reversal in the direction at about 2018 UT. During the active period the AA varies from -0.5 to 0.9.

Figures 2c and 2e show the radial and azimuthal projections of the AA for event 2. During the growth phase (before 1935 UT), $A_V$ and $A_D$ are more disturbed for event 2 than event 1. This is to be expected because for event 2 another substorm occurred earlier at 1917 UT. As for event 1, after 1935 UT, $A_V$, and to a lesser extent $A_D$, present oscillations with large amplitudes typically 5 times larger (for $A_V$) than during the growth phase. In the next section we compare the AA variation in the $V$ and $D$ directions with the drift velocity deduced from $E$ field measurements.

### 2.5. Comparison Between Electric Drift and Ion Flow Directions Deduced From Azimuthal Asymmetry

Assuming that the ion distribution function is a shifted Maxwellian with an average velocity $v_{av}$, the AA is related to the ratio $v_{av}/v_{th}$. The sign of the asymmetry gives the direction of the flow and can be compared with the measured electric drift. Figures 1 and 2 show that the AA of the integral ion flux, projected along $V$ (Figures 1c and 2c), exhibits the same variations as the $V$ component of the drift during the active phases (Figures 1b and 2b). The AA along $D$ ($A_D$) is more disturbed and seems to be shifted westward, as compared to the corresponding electric field component, for both events 1 and 2 (see Figures 1d, 1e, 2d, and 2e). As suggested above, this shift is likely to result from earthward directed pressure gradients. The large-amplitude fluctuations of $A_D$ during the active phase, however, show the same kind of behavior as the projection, along $D$, of the electric drift velocity. Given the uncertainties in the two types of measurements, the agreement is reasonably good. This comparison suggests that the flux asymmetry, described in the previous subsection is mostly associated with rapidly varying electric drifts, at

least during the active periods. Therefore during active periods and only on short timescales (timescales corresponding to large electric field bursts), the flow velocity is given by the electric drift.

The AA displayed in Figures 1c, 1e, 2c, and 2e contains short periods, indicated by shaded areas, where data are contaminated by large parallel flows. For instance at early breakup (event 2), during the first minute (1934-1935 UT), $A_V$ becomes sharply negative twice during a few tens of seconds, before $\mathbf{E}\times\mathbf{B}$ changes. Careful examination of the data shows that this early increase in $A_V$ is an artefact. In order to improve the statistical significance of the measured AA, we have integrated the flux over a relatively wide pitch angle range ($60° - 120°$) in each azimuthal bin. This procedure is valid as long as the pitch angle distribution is relatively flat around 90°. This was indeed the case, except for short time intervals (a few tens of seconds), in particular between 1934 and 1935 UT, when the ion distribution has a strong pitch angle anisotropy corresponding to magnetic field-aligned earthward flowing ions. In order to confirm the above interpretation, we have plotted the AA (not shown) over a narrower pitch angle range ($80° - 100°$). During periods of strong parallel ion flows, noted by shaded areas in Figures 1 and 2, the AA obtained with a narrower pitch angle range is indeed quite different from what is obtained with a wide pitch angle. Hence these periods have been excluded, as suggested by the shaded areas. As indicated above, this reduction in the pitch angle range, however, leads to an increase in the statistical fluctuations of the flux.

The electric drift $\mathbf{V}_E$ can be used to estimate, via a simple model, the AA this flow can produce. For a Maxwellian ion distribution the modulation $A$ of particles with velocity $V_0$ for a drift flow velocity $V_E$ can be written $A = 2\tanh(2V_EV_0/V_{th}^2)$. With a temperature $1/2mV_{th}^2 = 10$ keV, the rate of modulation of the flux of $1/2mV_0^2 = 30$ keV ions with velocity $V_0$, in the presence of a 100 km s$^{-1}$ electric drift velocity, is given by $A = 2\tanh(2V_EV_0/V_{th}^2) = 2\tanh(0.25) \simeq 0.5$, which fits with the observed modulation. Thus, even if $V_E/V_{th}$ is small, the AA can be quite large.

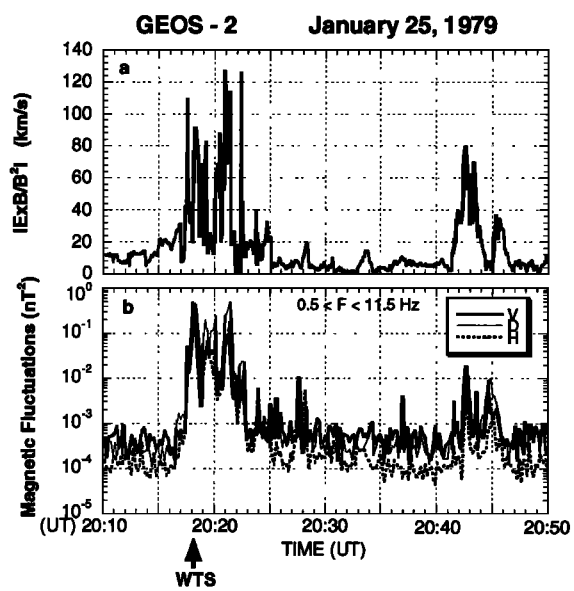


**Figure 3.** For January 25, 1979, (a) the modulus of the electric drift velocity $\mathbf{V_E} = \mathbf{E}\times\mathbf{B}/B^2$ and (b) the power of the current-driven Alfvén (CDA) waves, integrated between 0.5 Hz and 11 Hz.

Thus the radial ion flux modulation observed during the active phase can be accounted for by a radial electric drift velocity. The agreement between the two different evaluations confirms the existence of large transient flows during the active phase. Even if flow bursts can be found in any directions, the earthward direction prevails, on average, at least for event 1. Thus in the NEPS the earthward transport essentially occurs during the active phase, at and just after the substorm onset. Before breakup, during the growth phase, the electric field is usually weak, and the radial transport in particular, if any, is slow.

## 3. Relation Between Fast Flows and ULF Turbulence

The results presented in the previous section suggest the existence of two regimes of transport: (1) a slow transport during the growth phase and (2) a fast transient transport, during the active phase, at and just after the substorm onset. In the present section we investigate the possible relation between the plasma transport and the ultra low-frequency (ULF) waves which are regularly observed during the active phase of substorms [*Perraut et al.*, 1998, 2000]. Given that these waves are associated with magnetic signatures of small-scale currents, we call them current-driven Alfvén (CDA) waves [*Perraut et al.*, 2000].

Figure 3 illustrates the two transport regimes indicated above: Before and after the active phase, the modulus of the electric drift velocity is usually weak (Figure 3a), while during the active phase from about 2017 UT to 2022 UT, fast flow bursts are observed when (and only when) the power of the magnetic fluctuations illustrated in Figure 3b (the CDA waves) is large.

For event 2, Figure 4, the behavior of the two curves is also similar, though there is not necessarily a one-to-one correspondence between the peaks in the drift velocity and the peaks in the power of the CDA waves. For events 1 and 2, as well as for other dispersionless events observed in the NEPS, on GEOS 2, fast flow bursts are observed during the active phase of substorms, when the power of CDA waves is large, typically above $\sim 0.1$ nT$^2$. Notice that the background level is 2 orders of magnitude below, that is, $\sim 0.001$ nT$^2$. Conversely, when the power of CDA waves is weak, the electric field is small and steady; in particular, the azimuthal component $E_D$ is small, and therefore the radial transport is slow. Thus the level of CDA waves seems to correlate with the regime of transport. One should notice

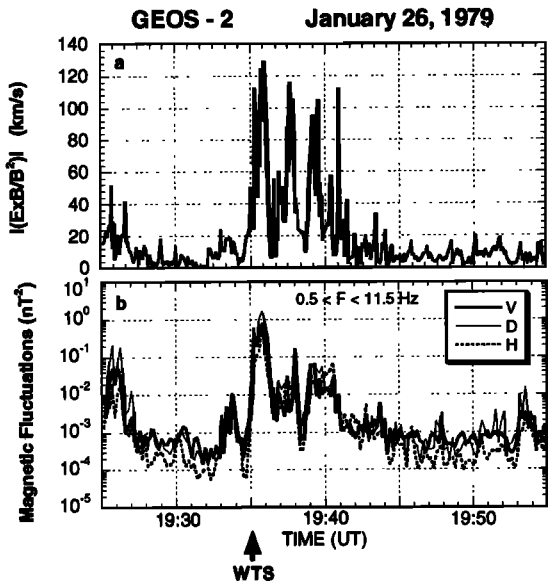


**Figure 4.** Same as Figure 3 for January 26, 1979.

that the relatively large drift velocities which do not correspond to a substorm onset, around 2043 UT for event 1 and around 1926 UT for event 2, are also correlated with a consistent AA variation (see Figures 1c and 2c) and to a relatively high level of the CDA waves (see Figures 3b and 4b). During these short periods the power in CDA waves, however, is less intense than during substorms, but still 1 or 2 orders of magnitude above the noise. They do not drive a global reconfiguration of the magnetic field. They are likely to be associated with smaller-scale (e.g., spatially confined) perturbations, possibly pseudobreakups. Therefore a correlation between convective flows and CDA waves seems to exist at different scales.

## 4. Discussion and Interpretation

We have found that in the NEPS, during the substorm growth phase (as well as after the active phase), $E_D$ and $E_V$, the azimuthal and radial components of the electric field, are generally weak and steady, close to the equator; there is little $\mathbf{E}\times\mathbf{B}/B^2$ transport. Conversely, fast (typically 100 km s$^{-1}$) transient flows coincide with substorm breakup (and pseudobreakup), and last about 5 min, during the active phase. These fast flows are not necessarily directed earthward and westward; reversals in the flow direction are frequent. This suggests that there are indeed two regimes of transport, as conjectured by *Kennel* [1995].

The agreement between the electric drift and $A_D$ is less good, however, than in the radial direction ($A_V$), which is presumably due to the simultaneous existence of a radial gradient in ion pressure. As discussed above, in subsection 2.4, owing to the lack of measurements of the differential intensities with the appropriate time resolution, we cannot distinguish between the signatures of a radial ion pressure gradient and that of an azimuthal flow (upon $A_D$).

In the present section we use the linear kinetic formalism introduced by *Pellat* [1990] for collisionless plasmas confined in a mirror geometry and developed by *Le Contel et al.* [2000a, 2000b] for the adiabatic plasma of the NEPS, in order to understand why the transport is so slow during the growth phase, and suddenly becomes fast during the active phase. To the lowest order in the electron to ion temperature ratio $T_e/T_i$ ($T_e/T_i \to 0$), *Le Contel et al.* [2000a] found that the enforcement of the quasi-neutrality condition (QNC) implies the development of an electrostatic potential $\Phi_0$ which is constant along the field lines, but varies across them, so that the potential $\mathbf{E}$ field is perpendicular to $\mathbf{B}$. This electrostatic potential $\Phi_0$ represents the self-consistent nonlocal (i.e., bounce-averaged) response of the plasma to an externally applied time-varying perturbation. Being nonlocal, this effect can not be described by MHD models. The important point in the present context is that the potential electric field tends to reduce the effect of the induced electric field associated with an applied perturbation, as shown in the next subsection. The result is a partial electric field shielding reducing the plasma flow which would have been produced by the induced electric field alone. Thus the electric field (i.e., induced plus potential) varies with latitude [*Le Contel et al.*, 2000a]. In the next subsection we summarize the results already obtained by *Le Contel et al.* [2000a] on the azimuthal electric field and use the same method to derive the radial component.

### 4.1. Self-Consistent Quasi-Static Perpendicular Electric Field

Local field-aligned coordinates defined by the triad of unit vectors

$$\mathbf{e}_\chi = \frac{\mathbf{B}}{B},\ \mathbf{e}_\psi = \frac{\nabla\psi}{|\nabla\psi|},\ \mathbf{e}_y = \mathbf{e}_\chi \times \mathbf{e}_\psi, \qquad (1)$$

with $\psi$ the flux function defined by $\mathbf{B} = \nabla\psi \times \mathbf{e}_y$ are used ($\mathbf{e}_\psi$ is directed radially outward as $V$ and $\mathbf{e}_y$ is directed eastward as $D$). We assume that the electromagnetic perturbation is periodic in time ($t$) and in space (in the $y$ direction)

$$\delta\mathbf{A}(\mathbf{r},t) \propto \widehat{\delta\mathbf{A}}(\psi,k_y,l,\omega,)\exp\left[i(k_y y+\omega t)\right], \qquad (2)$$

where $\mathbf{r}$ and $k_y$ are the position vector and the $y$ component of the wave vector, respectively, and $l$ is the distance along the magnetic field line (for the sake of simplicity we omit the hat symbol and the exponential factor in the following formulas). With these assumptions, *Hurricane et al.* [1995] showed that the radial and the azimuthal components of the electric field associated with low-frequency perturbations $\omega < \omega_{b,i}, \omega_{b,e}$ ($\omega_{b,i}, \omega_{b,e}$ being the bounce frequencies of ions and electrons, respectively) can be written as

$$\delta E_\psi = -B\frac{\partial}{\partial\psi}\left(\Phi_0(\lambda)-\lambda\right) - i\omega\delta A_\psi, \quad (3)$$

$$\delta E_y = -ik_y\left(\Phi_0(\lambda)-\lambda\right), \quad (4)$$

where $\lambda = i\omega\int^l dl'\delta A_\parallel$ and $\Phi_0$ is an electrostatic potential which is constant for a given magnetic field line; it is imposed by the quasi-neutrality condition. One should notice, however, that to obtain the full structure of the electric field along the field line, one needs to solve the full Vlasov/Maxwell system of equations for a finite frequency. This is a very hard task considering that for $\omega < \omega_{b,e}\omega_{b,i}$, the fluid approach is not valid. *Le Contel et al.* [2000a] obtained the azimuthal electric field in the quasi-static limit ($\omega < \omega_{b,i}, \omega_{b,e}$ and $\omega < k_\parallel v_A$, $k_\parallel$ being the parallel component of the wave vector and $v_A$ being the Alfvén velocity). They modeled the substorm growth phase in the near-Earth plasma sheet as a quasi-static magnetic field perturbation. They used the two-dimensional dipole to describe the quasi-dipolar region, neglected the local currents to the lowest order (low $\beta$ assumption, $\beta$ being the ratio between the plasma pressure and the magnetic field pressure), and computed self-consistently the magnetic field perturbations produced by an external current flowing farther in the tail. They solved the linearized Ampère's equation with a forcing current $\nabla\times\delta\mathbf{B} = \mu_0\delta j_{ext}\mathbf{e_y}$ localized in the radial and azimuthal directions, and corresponding to a current flowing in the western direction close to equator. This forcing current is written as

$$\delta j_{ext}(L,k_y,\theta,\omega) = \delta j_{eq}(k_y,\omega)\delta(L-L_c)\sin^{2n}\theta \cdot\left[(2n+1)\cot^2\theta - 1\right], \quad (5)$$

where $\theta$ is the colatitude and $L$ is the equatorial crossing distance of the relevant field line. We have chosen a class of forcing currents which corresponds to an increase in the equatorial current and still allows a simple derivation of the magnetic field perturbation. This class is labeled by an index $n$; the larger $n$ is, the more the perturbation is localized close to the magnetic equator (see *Le Contel et al.* [2000a] for more details). In the limit $|k_y|L > 1$ (which is equivalent to assuming that the characteristic scale of the perturbation along the $y$ direction is shorter than the characteristic scale of the equilibrium magnetic field in the radial direction), they computed the azimuthal (east/west) electric field associated with the magnetic field line stretching, which after an inverse Fourier transform can be written

$$\delta E_y = -\frac{\mu_0\delta j_m}{2(n+1)}L_c^2\gamma\exp(\gamma t)\frac{L}{d}\frac{1}{\sqrt{\pi}} \cdot\left[S_n - \left(\sin^2\theta\right)^{n+1}\right]\left\{1+\zeta Pf\left[\tilde{W}(\zeta)\right]\right\}, \quad (6)$$

where $Pf$ is the Cauchy principal value and $\tilde{W}(\zeta) = 1/(\sqrt{\pi})\int_{-\infty}^{\infty}dV\exp(-V^2)/(V-\zeta)$ is the Fried-Conte function (with $V = y'/d$ and $\zeta = y/d$). To derive (6), they assumed that $\delta j_{eq}(y,t) = \delta j_m\exp(-y^2/d^2)\exp(\gamma t)$, where $d$ is the scale length of the current sheet in the $y$ direction and $1/\gamma$ is the characteristic timescale of the growth phase.

In this paper we present the calculation of the radial component of the electric field which develops in the quasi-dipolar region, in response to the increase of the azimuthal current farther in the tail. Following *Le Contel et al.* [2000a] and in the same limit $|k_y|L > 1$ (see Appendix A), we obtain

$$\delta E_\psi = \frac{\mu_0\delta j_m}{4}L_c^2\frac{L}{d}\gamma\exp(\gamma t)\left\{\frac{B}{B_{eq}} \cdot\left[\frac{d}{L}\frac{Pf\left[W(\zeta)\right]}{\pi^{1/2}}\frac{S_n-(\sin^2\theta)^{n+1}}{n+1} + 2\frac{y}{d}\exp\left(-\frac{y^2}{d^2}\right) \cdot\left\{H(L-L_c)-H\left[-(L-L_c)\right]\right\}\frac{S_{n+1}-(\sin^2\theta)^{n+2}}{n+2}\right] -\pi^{1/2}\left(\frac{d}{L}\right)^2 erf(\zeta)\sin^{2n}\theta\Big((2n+1)-(2n+2)\sin^2\theta\Big) \cdot\Big\{H(L-L_c)-H\left[-(L-L_c)\right]\Big\}\Big\}, \quad (7)$$

where $H(L)$ stands for the Heaviside function. We consider the region earthward of the location of the external current ($\{H(L-L_c)-H\left[-(L-L_c)\right]\} = -1$) and to simplify we assume that we are close to the noon-midnight meridian ($\zeta = y/d < 1$). Therefore it is convenient to define the following nondimensional electric fields:

$$\delta\tilde{E}_y = \frac{\delta E_y}{\delta E_a} \simeq F_n(\theta), \quad (8)$$

$$\delta\tilde{E}_\psi = \frac{\delta E_\psi}{\delta E_a} \simeq G_n(\theta)\left(\frac{y}{d}\right), \quad (9)$$

where

$$\delta E_a = \mu_0\delta j_m L_c^2\frac{L}{2d}\gamma\exp(\gamma t), \quad (10)$$

and

$$F_n(\theta) = -\frac{1}{\sqrt{\pi}}\frac{1}{n+1}\left[S_n - \left(\sin^2\theta\right)^{n+1}\right], \quad (11)$$

$$G_n(\theta) = -\frac{1}{\sin^2\theta}\left[\frac{S_{n+1}-\left(\sin^2\theta\right)^{n+2}}{n+2} + \frac{d}{L}\frac{S_n-\left(\sin^2\theta\right)^{n+1}}{(n+1)\sqrt{\pi}}\right] + 2\left(\frac{d}{L}\right)^2\sin^{2n}\theta \cdot\left[(2n+1)-(2n+2)\sin^2\theta\right], \quad (12)$$

where $S_n$ is given by (A9) in Appendix A. The variations of $\delta\tilde{E}_y$ and $\delta\tilde{E}_\psi$ along the magnetic field line are plotted in Figure 5 for $n = 0$ and $y/d = 1/2$. We see that close to the equator ($\theta \simeq \pi/2$), $\delta\tilde{E}_y$ and $\delta\tilde{E}_\psi$ are small. Therefore owing to the existence of the electrostatic potential $\Phi_0$ ($\Phi_0$ corresponds to $S_n$ and $S_{n+1}$ in the formulas (11) and (12), respectively), the motion

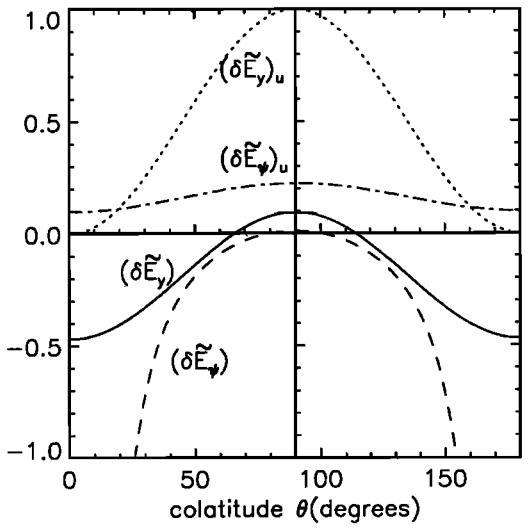


**Figure 5.** Normalized values of the azimuthal ($\delta\widetilde{E}_y$) and radial ($\delta\widetilde{E}_\psi$) components of the quasi-static electric field as functions of the colatitude $\theta$. For the sake of comparison, unshielded components $(\delta\widetilde{E}_y)_u$ and $(\delta\widetilde{E}_\psi)_u$ are also plotted.

of the equatorial particles is small during the growth phase. At middle-colatitudes ($\theta \simeq 45°$), the azimuthal and radial components are comparable. Note that $\delta\widetilde{E}_\psi$ changes direction from dawnside to duskside. To show the effect of the cancellation of the shielding effect associated with $\Phi_0$, we have plotted in Figure 5 also $(\delta\widetilde{E}_y)_u$ and $(\delta\widetilde{E}_\psi)_u$, the variations of the azimuthal and radial components of the unshielded electric field, that is, when $S_0 = S_1 = 0$. We note that close to the equator, both the azimuthal and the radial components of the unshielded electric field are typically 1 order of magnitude larger than in the shielded case. In the next section we discuss why such a cancellation of the shielding effect may occur at substorm onset.

### 4.2. Shielded Electric Field: Numerical Estimates

During the growth phase, in the near-Earth quasi-dipolar magnetic field ($X \leq 10\ R_E$), for magnetic field variations corresponding to the formation of a current sheet ($B_H \searrow$ and $|B_V| \nearrow$), the (total) electric field displayed in Figure 5 is (in the duskside): (1) directed eastward and earthward (but partially shielded), near the equator, (2) null (completely shielded) at some distance away from the magnetic equator (near the boundary of the current sheet), and (3) westward and tailward away from the equator. Notice that at high latitudes, the electrostatic component dominates and produces an earthward and westward transport during the growth phase. Thus for a time-dependent transport in the dusk sector (1) large equatorial pitch angle particles, confined near the equator, drift tailward and eastward whereas small pitch angle particles spend most of their time at high latitudes, and therefore drift earthward and westward, and (2) the equatorial electric field cannot be mapped onto the ionosphere, even in the absence of a parallel electric field.

For the two events discussed here, we can estimate from Faraday's law the magnitude of the expected induced electric field associated with the stretching of the magnetic field lines. For event 1 we have $\Delta E_y \simeq \Delta B_z \Delta X/\Delta t \simeq 0.1$ mV m$^{-1}$ with $\Delta B_z \simeq \Delta B_H \simeq 10$ nT, $\Delta t \simeq 1/\gamma \simeq 40$ min, and $\Delta X \simeq 4\ R_E$ (see Figure 5 of *Roux et al.* [1991], which displays the total duration of the growth phase). For this event the magnetic field varies slowly during the growth phase; therefore the induced electric field is in the range of the error bar ($\pm 0.5$ mV m$^{-1}$) of the spherical double probes on GEOS 2 [*Pedersen et al.*, 1985]. Yet, for event 2 we obtain $\Delta E_y \simeq 1.5$ mV m$^{-1}$ with $\Delta B_z \simeq \Delta B_H \simeq 35$ nT, $\Delta t \simeq 1/\gamma \simeq 10$ min, and $\Delta X \simeq 4\ R_E$. Using formula (26) of *Le Contel et al.* [2000a], which relates $\delta B_\parallel \simeq \Delta B_H$ to the forcing current, we obtain $\delta j_m \simeq 2\delta B_\parallel L/\mu_0 L_c^2 \simeq 1.23 \times 10^{-10}$ A m$^{-2}$ for event 1 and $\delta j_m \simeq 4.3 \times 10^{-10}$ A m$^{-2}$ for event 2, where for both events we have assumed that $L_C = 7\ R_E$ and $L = 6.6\ R_E$. Assuming that $d$, the scale length of the current sheet in the $y$ direction, is equal to 4 $R_E$ in equation (10), we obtain $\delta E_a \simeq 0.3$ mV m$^{-1}$ for event 1 and $\delta E_a \simeq 4$ mV m$^{-1}$ for event 2, which are equivalent to previous estimates if we take into account the variation with the colatitude (see Figure 5). For event 2 the estimated radial electric drift $\Delta V_E \simeq \Delta E_y/B \simeq 30$ km s$^{-1}$ with $B \simeq 70$ nT should be observable, but is not observed, as can be seen in Figure 4. The same comment can be made for the azimuthal electric drift. However, if the spacecraft is near the boundary of the current sheet (the $B_V$ and $B_H$ components are of the same order of magnitude), the electrostatic field tends to cancel the induced component of the electric field. Thus we suggest that the shielding may explain the lack of plasma transport during the growth phase.

### 4.3. Unshielded $E$ Field: Fast Transport

Why is the situation different during the active phase? If, for some reason, "particle collisions" were to occur on timescales shorter than the bounce time, the bounce motion would be inhibited, and the nonlocal response would disappear. *Perraut et al.* [2000] have pointed out that pseudocollisions associated with CDA waves represent an efficient mechanism for diffusing electrons in velocity space (more precisely in $V_\parallel$). CDA waves may indeed have a finite parallel electric field. For $E_\parallel = 0.025 E_\perp$, and $E_\perp \sim 5$ mV m$^{-1}$ (as measured), one gets approximately $E_\parallel \sim 0.1$ mV m$^{-1}$. The corresponding diffusion coefficient $D_\parallel$ is given by

$$D_\parallel = \frac{\pi}{2}\left(\frac{e}{m_e}\right)^2 \frac{|E_\parallel\left(k_\parallel = \frac{\omega}{v_\parallel}\right)|^2}{\Delta k |v_\parallel - v_{g,\parallel}|} = 10^{14} \mathrm{m^2 s^{-3}},$$

where $\Delta k$ is the spectral width and $v_{g,\parallel}$ is the parallel group velocity. For 5 keV electrons (remember that the thermal energy of plasma sheet electrons is less than 5 keV), the diffusion time $T_d \simeq 10$ s is of the order of the bounce period (8 s). For energies below 5 keV, diffusion occurs over a faster timescale than the electron bounce period. This suggests a simple explanation for the control exerted by CDA waves on the properties of the transport. As soon as CDA waves are sufficiently intense to destroy the periodic bounce motion of electrons, (1) the parallel current is disrupted [*Perraut et al.*, 2000] and (2) the nonlocal term $\Phi_0$ cancels; the associated shielding vanishes. Then, the azimuthal $E_D$ and radial $E_V$ electric fields become equal to the induced electric field associated with the magnetic field variations produced by the disruption of the parallel current; the disappearance of the shielding implies a strong enhancement of the azimuthal and radial electric fields, as observed. One should notice that during the quasi-periodic oscillations with 5 min period observed on the $B_H$ and $B_V$ components of the magnetic field for event 1 between 2025 UT and 2035 UT, no electric drifts are measured. Conversely, around 2043 UT, similar magnetic field variations on $B_H$ and $B_V$ give a large electric drift because a relatively high level of CDA waves is present. Similarly, an enhanced $\mathbf{E}\times\mathbf{B}/B^2$ drift is observed in association with enhanced CDA waves, around 1926 UT, in event 2. Thus large electric drifts associated with temporal magnetic field variations occur only on short timescales, and they are correlated with high levels of CDA waves.

To rigorously determine exactly the new mode structure of the electric field, we need to solve the Vlasov/Maxwell system of equations for a finite low-frequency perturbation ($\omega < \omega_{b,i}\omega_{b,e}$) with a new term describing the interaction with CDA waves. This task is outside the scope of this paper, but thanks to the quasi-static calculations presented here, we have been able to suggest a mechanism which permits the existence of large electric fields.

## 5. Summary and Conclusions

Field and particle measurements, carried out in the NEPS, have been used as evidence for two regimes of plasma transport:

1. During the growth phase, and after the end of the active phase (the active phase being characterized by arcs/surges activated near the magnetic footprint of GEOS 2), the azimuthal and radial electric fields, and hence the radial and azimuthal electric drift velocities, are small and steady even when long-period (200 s) perturbations occur in the magnetic field (see event 1 between 2025 UT and 2035 UT). These slow drifts are interpreted as a consequence of the electrostatic shielding of the induced electric field associated with time-varying external conditions. The electrostatic shielding is a nonlocal (nonMHD) effect, produced by electron bouncing along magnetic field lines.

2. During the active periods, in particular at breakup, large-amplitude flow bursts, with typical velocities of $\sim 100\ \mathrm{km\,s^{-1}}$, are observed. These flow bursts are associated with intense low-frequency electromagnetic fluctuations: current-driven Alfvén waves (CDA waves). Once their power is large enough, CDA waves produce a diffusion in velocity space on a timescale shorter than the bounce period. Even for modest parallel electric fields ($E_\parallel \simeq 0.1\ \mathrm{mV\ m^{-1}} \ll E_\perp \simeq 1-10\ \mathrm{mV\ m^{-1}}$), the diffusion time is shorter than the bounce period for electrons with energies below 5 keV. This fast diffusion is equivalent to "anomalous" collisions that violate the conservation of the second adiabatic invariant for electrons, thereby destroying the electrostatic shielding associated with the electron bounce motion. When the shielding is cancelled on short timescales (shorter than the electron bounce period), the total electric field is only given by the induced electric field which accompanies the magnetic topology change; therefore a sudden fast convective motion of the plasma occurs. We point out that this mechanism seems to be efficient during substorms as well as during small-scale perturbations (pseudosubstorm); in the latter case the level of the power of CDA waves is lower. Thus a microscopic process, electron diffusion in velocity space, may control the large-scale (as well as the small-scale) plasma transport in the NEPS. Finally, one may wonder whether the fast flows observed in the NEPS are the same kind of event as those observed farther out in the tail. Typical speeds found in NEPS are $100\ \mathrm{km\,s^{-1}}$ for substorm events, which is 5 to 10 times smaller than fast flows observed at about 20 $R_E$. This factor (5 to 10), however, is nothing but the ratio between the average magnetic fields at 7 $R_E$ ($\simeq 80$ nT) and at 20 $R_E$ ($\simeq$ 10-15 nT). The size of the azimuthal $E$ field spikes is the same.

## Appendix A: Calculation of the Radial Electric Field

The calculation of the radial electric field is more difficult than that of the azimuthal electric field because we cannot assume a periodic dependence of the solution in the radial direction. The radial electric field can be written as

$$\delta E_\psi = -B\frac{\partial}{\partial\psi}\delta\Phi - \frac{\partial}{\partial t}\delta A_\psi, \qquad \text{(A1)}$$

with $\delta\Phi = \Phi_0(\lambda) - \lambda$, where $\Phi_0$ is a constant part of the perturbed electrostatic potential imposed by the quasi-neutrality condition; the expression for $\Phi_0$ is given by equation (13) of *Le Contel et al.* [2000a]. As in the work by *Le Contel et al.* [2000a], we assume that the perturbation varies faster than the equilibrium; therefore we can interchange the $\psi$ derivative and the integration on $l$ in the expression for $\Phi_0$ and write

$$\delta E_\psi = -B\left(\Phi_0\left(\frac{\partial}{\partial\psi}\lambda\right) - \frac{\partial}{\partial\psi}\lambda\right) - \frac{\partial}{\partial t}\delta A_\psi. \qquad \text{(A2)}$$

In the following we calculate successively the two com-

ponents of the $E$ field, namely, the electrostatic component $\delta E_\psi^{e.s}$ and the induced component $\delta E_\psi^{ind}$. First, we compute $\delta E_\psi^{e.s}$. To correctly perform the $\psi$ derivative of $\lambda$, we need to return to the solution of Ampère's equation obtained by *Le Contel et al.* [2000a]; it is written

$$\lambda_n(L,k_y,\theta,\omega)=\frac{\mu_0}{4}\frac{\omega|k_y|}{k_y}\delta j_{eq}(k_y,\omega)L_c^2L \cdot\int duu^n\exp(Zu), \quad \text{(A3)}$$

where we have defined $u=\sin^2\theta$ and $Z=-|k_y(L-L_c)|$. In a two-dimensional dipole, we have $d\psi=B_{eq}dL$, which yields

$$B\frac{\partial}{\partial\psi}\lambda=\frac{B}{B_{eq}}\frac{\mu_0}{4}\frac{\omega|k_y|}{k_y}\delta j_{eq}(k_y,\omega)L_c^2L \cdot\left[\int duu^n\exp(Zu)+L\frac{\partial Z}{\partial L}\int duu^{n+1}\exp(Zu)\right]. \quad \text{(A4)}$$

We obtain

$$B\frac{\partial}{\partial\psi}\lambda=\frac{B}{B_{eq}}\frac{\mu_0}{4}\frac{\omega|k_y|}{k_y}\delta j_{eq}(k_y,\omega)L_c^2L\Big[F_n(Z,u) -|k_y|L\left\{H(L-L_c)-H\left[-(L-L_c)\right]\right\}F_{n+1}(Z,u)\Big], \quad \text{(A5)}$$

where we have defined

$$F_n(Z,u)=\int duu^n\exp(Zu)=\left[u^n/Z+\sum_{k=1}^{n}(-1)^k n(n-1)\ldots(n-k+1)u^{n-k}/Z^{k+1}\right]\exp(Zu), \quad \text{(A6)}$$

and $H(L)$ stands for the Heaviside function. One can show that for $Z=-|k_y(L-L_c)|<1$, which implies that the wavelength of the perturbation is larger than the distance between the current and the location where the solution is calculated, we have $F_n(Z,u)\simeq n!/Z^{n+1}+u^{n+1}/(n+1)$, and we obtain

$$B\frac{\partial}{\partial\psi}\lambda=\frac{B}{B_{eq}}\frac{\mu_0}{4}\frac{\omega|k_y|}{k_y}\delta j_{eq}(k_y,\omega)L_c^2L\left[\frac{n!}{Z^{n+1}}+\frac{u^{n+1}}{n+1}-|k_y|L\Big\{H(L-L_c)-H\left[-(L-L_c)\right]\Big\}\left(\frac{(n+1)!}{Z^{n+2}}+\frac{u^{n+2}}{n+2}\right)\right]. \quad \text{(A7)}$$

Keeping in mind that $\delta E_\psi^{e.s}=B\partial/\partial\psi(\Phi_0-\lambda)$, and taking into account the expression for $\Phi_0$ given in Appendix D of *Le Contel et al.* [2000a], the electrostatic part of the electric field becomes

$$\delta E_\psi^{e.s}=\frac{B}{B_{eq}}\frac{\mu_0}{4}\frac{\omega|k_y|}{k_y}\delta j_{eq}(k_y,\omega)L_c^2L \cdot\left[\frac{S_n-(\sin^2\theta)^{n+1}}{n+1}-|k_y|L\Big\{H(L-L_c)-H\left[-(L-L_c)\right]\Big\}\frac{S_{n+1}-(\sin^2\theta)^{n+2}}{n+2}\right], \quad \text{(A8)}$$

where we have defined

$$S_n=\sum_{k=0}^{n+1}(-1)^k C_{n+1}^k\frac{(2k-1)!!}{(2k+2)!!} \cdot\sum_{j=0}^{k}(-1)^j C_k^j\frac{(2j)!!}{2^{j-1}(j+1)!}\left(1+k\frac{j+1}{j+2}\right). \quad \text{(A9)}$$

We perform the inverse Fourier transform, which yields (see Appendix B of *Le Contel et al.* [2000a] for a similar derivation)

$$\delta E_\psi^{e.s}(L,y,\theta,t)=\frac{B}{B_{eq}}\frac{\mu_0\delta j_m}{4}L_c^2\gamma\exp(\gamma t)\frac{L}{d} \cdot\left[\frac{d}{L}\frac{W(\zeta)}{\pi^{1/2}}\frac{S_n-(\sin^2\theta)^{n+1}}{n+1}+2\frac{y}{d}\exp\left(-\frac{y^2}{d^2}\right)\Big\{H(L-L_c)-H\left[-(L-L_c)\right]\Big\}\frac{S_{n+1}-(\sin^2\theta)^{n+2}}{n+2}\right], \quad \text{(A10)}$$

where $\tilde{W}(\zeta)=1/(\sqrt{\pi})\int_{-\infty}^{\infty}dV\exp(-V^2)/(V-\zeta)$ is the Fried-Conte function and we have defined $V=y'/d$ and $\zeta=y/d$.

Now, we compute the inductive part of the radial electric field, which is witten $\delta E_\psi^{ind}=-i\omega\delta A_\psi=\omega/k_y\delta B_\parallel$. From equation (A27) in Appendix A of *Le Contel et al.* [2000a], we obtain

$$\delta E_\psi^{ind}(L,k_y,\theta,\omega)=-\frac{\omega}{k_y}\frac{\mu_0\delta j_{eq}(k_y,\omega)}{2}\frac{L_c^2}{L}\sin^{2n}\theta \cdot\Big((2n+1)-(2n+2)\sin^2\theta\Big)\Big\{H(L-L_c)-H\left[-(L-L_c)\right]\Big\}. \quad \text{(A11)}$$

After an inverse Fourier transform we get

$$\delta E_\psi^{ind}(L,y,\theta,t)=-\pi^{1/2}\frac{\mu_0\delta j_m}{4}L_c^2\frac{d}{L}\gamma\exp(\gamma t) \cdot\mathrm{erf}(\zeta)\sin^{2n}\theta\Big((2n+1)-(2n+2)\sin^2\theta\Big)\Big\{H(L-L_c)-H\left[-(L-L_c)\right]\Big\},$$

where we have defined $\mathrm{erf}(\zeta)=2/\pi^{1/2}\int_0^\zeta\exp-x^2dx$.

The total radial electric field $\delta E_\psi=\delta E_\psi^{e.s}+\delta E_\psi^{ind}$ becomes

$$\delta E_\psi = \frac{\mu_0 \delta j_m}{4} L_c^2 \frac{L}{d} \gamma \exp(\gamma t) \left\{ \frac{B}{B_{eq}} \cdot \left[ \frac{d}{L} \frac{W(\zeta)}{\pi^{1/2}} \frac{S_n - (\sin^2\theta)^{n+1}}{n+1} + 2\frac{y}{d} \exp\left(-\frac{y^2}{d^2}\right) \cdot \left\{ H(L-L_c) - H\left[-(L-L_c)\right] \right\} \frac{S_{n+1} - (\sin^2\theta)^{n+2}}{n+2} \right] - \pi^{1/2} \left(\frac{d}{L}\right)^2 \operatorname{erf}(\zeta) \sin^{2n}\theta \left( (2n+1) - (2n+2)\sin^2\theta \right) \cdot \left\{ H(L-L_c) - H\left[-(L-L_c)\right] \right\} \right\}. \quad \text{(A12)}$$

**Acknowledgments.** Michel Blanc thanks the two referees for their assistance in evaluating this paper.

## References


Angelopoulos, V., W. Baumjohann, C. F. Kennel, F. V. Coroniti, M. G. Kivelson, R. Pellat, R. J. Walker, H. Lühr, and G. Paschmann, Bursty bulk flows in the inner central plasma sheet, *J. Geophys. Res.*, *97*, 4027, 1992.

Hurricane, O. A., R. Pellat, and F. V. Coroniti, A new approach to low-frequency "mhd-like" waves in magnetospheric plasmas, *J. Geophys. Res.*, *100*, 19,421, 1995.

Kennel, C. F., *Convection and Substorms*, Oxford Univ. Press, New York, 1995.

Knott, K., Payload of the GEOS scientific geostationary satellite, *ESA Sci. Tech. Rev.*, *1*, 173, 1975.

Korth, A., G. Kremser, and B. Wilken, Observations of substorm-associated particle-flux variations at $6 \leq l \leq 8$ with GEOS-1, *Space Sci. Rev.*, *22*, 501, 1978.

Le Contel, O., R. Pellat, and A. Roux, Self-consistent quasi-static radial transport during the substorm growth phase, *J. Geophys. Res.*, *105*, 12,929, 2000a.

Le Contel, O., R. Pellat, and A. Roux, Self-consistent quasi-static parallel electric field associated with substorm growth phase, *J. Geophys. Res.*, *105*, 12,945, 2000b.

Lui, A. T., et al., Current disruption in the near-Earth neutral sheet region, *J. Geophys. Res.*, *97*, 1461, 1992.

Lui, A. T., A. Mankofsky, C. L. Chang, K. Papadopoulos, and C. S. Wu, A current disruption mechanism in the neutral sheet: A possible trigger for substorm expansions, *Geophys. Res. Lett.*, *17*, 745, 1990.

Mitchell, D. G., R. Lundin, and D. J. Williams, Analyses of convective flows and spatial gradients in energetic ion observations, *J. Geophys. Res.*, *91*, 8827, 1986.

Nakamura, T., D. N. Baker, D. H. Fairfield, D. G. Mitchell, R. L. McPherron, and E. W. Hones Jr., Plasma flow and magnetic field characteristics near the midtail neutral sheet, *J. Geophys. Res.*, *99*, 23,591, 1994.

Ohtani, S.-I., K. Takahashi, L. J. Zanetti, T. A. Potemra, R. W. McEntire, and T. Iijima, Initial signatures of magnetic field and energetic particle fluxes at tail reconfiguration: Explosive growth phase, *J. Geophys. Res.*, *97*, 19,311, 1992.

Pedersen, A., C. A. Cattel, C.-G. Fälthammar, K. Knott, P.-A. Lindqvist, R. H. Manka, and F. S. Mozer, Electric fields in the plasma sheet and plasma sheet boundary layer, *J. Geophys. Res.*, *90*, 1231, 1985.

Pellat, R., Une nouvelle approche de la reconnexion magnétique: Sous-orages magnétosphériques - vents stellaires, *C. R. Acad. Sci.*, *311*, 1706, 1990.

Perraut, S., A. Morane, A. Roux, A. Pedersen, R. Schmidt, A. Korth, G. Kremser, B. Aparicio, and R. Pellinen, Characterization of small scale turbulence observed at substorm onsets: Relationship with parallel acceleration of particles, *Adv. Space Res.*, *13*, 217, 1993.

Perraut, S., A. Roux, O. Le Contel, R. Pellat, A. Pedersen, and A. Korth, Evidence for a substorm trigger, in *Fourth International Conference on Substorms*, edited by S. Kokubun and Y. Kamide, p. 349, Kluwer Acad., Norwell, Mass., 1998.

Perraut, S., O. Le Contel, A. Roux, R. Pellat, A. Korth, Ø. Holter, and A. Pedersen, Disruption of parallel current at substorm breakup, *Geophys. Res. Lett.*, *27*, 4041, 2000.

Pu, Z. Y., A. Korth, and G. Kremser, Plasma and magnetic field parameters at substorm onsets derived from GEOS-2 observations, *J. Geophys. Res.*, *97*, 19,341, 1992.

Roux, A., et al., Plasma sheet instability related to the westward traveling surge, *J. Geophys. Res.*, *96*, 17,697, 1991.

Sauvaud, J.-A., and J. R. Winckler, Dynamics of plasma, energetic particles, and fields near synchronous orbit in the nighttime sector during magnetospheric substorms, *J. Geophys. Res.*, *85*, 2043, 1980.

Shinohara, I., T. Nagai, M. Fujimoto, T. Terasawa, T. Mukai, K. Tsuruda, and T. Yamamoto, Low-frequency electromagnetic turbulence observed near the substorm onset site, *J. Geophys. Res.*, *103*, 20,365, 1998.

Walker, R. J., K. N. Erickson, R. L. Swanson, and J. R. Winckler, Substorm-associated particle boundary motion at synchronous orbit, *J. Geophys. Res.*, *81*, 5541, 1976.



Ø. Holter and A. Pedersen, University of Oslo, Department of Physics, Boks 1048 Blindern, 0316 Oslo, Norway.

A. Korth, Max–Planck–Institut für Aeronomie, 37191 Katlenburg–Lindau, Germany.

O. Le Contel, S. Perraut and A. Roux, Centre d'Etude des Environnements Terrestre et Planétaires, 10–12 avenue de l'Europe, F–78140 Vélizy, France. (olivier.lecontel@cetp.ipsl.fr)

R. Pellat, Commissariat à l'Énergie Atomique, rue de la fédération, F–75007, Paris, France.


(Received February 28, 2000; revised January 11, 2001; accepted January 11, 2001.)